PERFORMANCE EVALUATION OF RESOLUTION RECOVERY IN 2D AND 3D PET DURING ITERATIVE IMAGE RECONSTRUCTION

E. De Bernardi*, F. Zito**, M. Mazzoli*, L. Mainardi*, P. Gerundini** and G. Baselli*

* Biomedical Engineering Department, Polytechnic University of Milan, Italy
** Nuclear Medicine Department, Ospedale Maggiore Policlinico, Mangiagalli e Regina Elena, Milan, Italy

Corresponding author: elisabetta.debernardi@polimi.it

Abstract: Aim of this work is the performance evaluation of spatial resolution recovery by means of iterative reconstruction in Positron Emission Tomography (PET). The algorithm properties in terms of contrast recovery, image noise and quantification accuracy have been evaluated on scanned phantom studies. Extensive comparisons of standard and resolution recovery algorithms, over wide parameter ranges with and without post-filtering are presented. Resolution recovery, by delaying noise breakup appearance and by increasing contrast, is able to improve counts spatial distribution accuracy for small objects and large blurring amount at clinical count statistics level, if reconstruction parameters are properly chosen.

Introduction

Spatial resolution in Positron Emission Tomography (PET) is mainly limited by positron range, annihilation gamma rays non collinearity, detector size, cross talk between adjacent crystals, and detector-photomultipliers coupling. Consequent partial volume and spillover effects on reconstructed images limit lesion detectability for small objects, accuracy in radiotracer concentration estimation and structures shape identification capacity. Furthermore, spatial resolution worsens at increasing distances from the scanner axis, thus making the resolution recovery item particularly important in oncological ^{18}F-FDG studies, where the detection and analysis of lesions overall the scanner Field Of View (FOV) is required.

The inclusion of scanner resolution degrading factors in the system matrix used by iterative reconstruction algorithms allows to recover spatial resolution during image reconstruction processes. This approach has been widely used in 2D and 3D whole body studies with different reconstruction algorithms, as in [1]. In our study we included the experimentally measured scanner transaxial blurring properties in the 2D Ordered Subset Expectation Maximization (OSEM) reconstruction algorithm [2]. In previous works [3,4] we assessed the algorithm capability to improve contrast without increasing noise component on cold and hot spot Jaszczak phantoms. In those studies, OSEM with and without including resolution recovery results were always compared using the same parameters, i.e. number of iterations, number of projection subsets and degree of post-filtering.

Aim of the present study is a deeper performance evaluation of the algorithm in order to define its own utility and also its limits in studies closer to clinical oncological condition. In this perspective, phantoms with hot spheres in hot background, in different conditions of contrast, blurring, and background uniformity, were used. A wide range of reconstruction parameters was systematically explored, in order to better study the effect of resolution recovery introduction inside OSEM. The evaluation was done in 2D and in 3D acquisition mode.

Materials and Methods

All data were acquired on a CTI-Siemens ECAT EXACT HR+ scanner (transaxial field of view 58.8cm, 144 angular projections sinogram with bin size 2.25mm). Software scatter correction was not applied to 3D data shown in this study.

LSF evaluation: The spatially variant Line Spread Function (LSF) was experimentally evaluated by means of an activity filled line source both with extended and retracted septa (2D and 3D acquisition mode). In 3D mode acquired data were rebinned with Fourier Rebinning algorithm (FORE), [5], and so its effect on transaxial spatial resolution was also considered. All the information about spatial resolution were included in the system matrix portion required by 2D OSEM image reconstruction.

Phantom studies: Two phantom studies were performed. The first one was a 20cm diameter cylinder filled with aqueous solution of ^{18}F and with 8 spheres of different internal radius (4.8, 5.1, 6.1, 6.2, 7.8. 11.0, 14.0 and 16.4mm). The phantom was scanned on axis and 15cm off axis in 2D mode. Two kinds of acquisition were performed: sphere to bkg activity ratio 7 and 14. The sphere phantom considered acquisitions are summarised in Table 1. In order quantitate the differences in the algorithm performance due only to sphere diameter to blurring amount ratio or to sphere to bkg activity ratio, the scan duration for the considered acquisitions was set in order to nearly obtain the same mean counts inside the biggest sphere (22counts/mm^3 after attenuation correction).

ISSN: 1727-1983

Table 1: Sphere phantom acquisitions.

	Acquisition mode	**Position**	**Contrast sphere/bkg**
2Don7	2D	On axis	7
2Doff7	2D	Off axis	7
2Don14	2D	On axis	14
2Doff14	2D	Off axis	14

The second phantom was the Alderson thorax-abdomen phantom with districts filled with different activity, simulating the in vivo ^{18}F-FDG uptake. Spherical lesions of different radii (2.1, 4.1, 5.1, 6.1, 11.0mm) were positioned inside. This phantom was scanned at a clinical counting statistics level (4min emission scan, 1min transmission post-injection scan) in 2D and 3D acquisition mode. Two acquisitions were performed in both the scanning conditions. The sphere to bkg activity ratio was 6 for all the spheres, except for the 2.1mm one (ratio 54). The background activity averaged round the lesions was used to measure the activity ratios.

Reconstruction algorithm: 2D data and 3D data after FORE rebinning were reconstructed with 2D OSEM in its Attenuation Weighted form (AWOSEM) with (REC) and without (NOREC) including LSF into the system matrix. In order to deeply analyze the algorithm performances, data were reconstructed at different iteration numbers (1-8) varying the number of subsets (4-72). The effect of changing sigma of post-reconstruction 2D Gaussian filter (0, 0.5, 0.75, 1, 1.25*pixel size) was also evaluated.

Figures of merit (FOMs): To quantitate image quality, Regions Of Interest (ROIs) were defined. Circular ROIs with radius equal to 70% of the sphere radius were drawn on each sphere of the two phantoms. For the sphere phantom, the background ROIs had all the same extension (140 pixels) and were placed around each sphere. For each sphere of the Alderson phantom instead, a square ROI of about 200 pixels was drawn on the nearest hot background. Three figures of merit were evaluated: CA, Contrast Accuracy, measured as:

$$CA = \frac{(\mu_{sphere} / \mu_{bkg} - 1)}{(a_{sphere} / a_{bkg} - 1)} \quad (1)$$

where μ_{sphere} and μ_{bkg} are the mean counts measured in the sphere ROI and in the corresponding background ROI; a_{sphere} and a_{bkg} are sphere and background activity, respectively. The noise component on the background was measured through the Noise to Signal Ratio (NSR) defined, for the sphere phantom, as:

$$NSR = \frac{s_{bkg}}{m_{bkg}} \quad (2)$$

where m_{bkg} and s_{bkg} are sample mean and standard deviation of counts measured over all the 8 background ROIs. For the Alderson phantom background ROIs were positioned in districts of different activity and then NSR was evaluated for each of the 5 ROI individually as:

$$NSR = \frac{\sigma_{bkg}}{\mu_{bkg}} \quad (3)$$

To evaluate object non uniformity degree due to reconstruction algorithm, variability was also measured for each sphere and defined as:

$$SV = \frac{\sigma_{sphere}}{\mu_{sphere}} \quad (4)$$

where μ_{sphere} and σ_{sphere} are sample mean and standard deviation of counts measured in the sphere ROI.

Finally, to give a score to AWOSEM-REC in respect to AWOSEM-NOREC in all the different considered physical conditions (sphere radius, activity contrast, blurring, acquisition mode), to better define its utility and limits, an unique FOM, able to summarise the information contained in the three previously defined FOMs, was needed. Because of the different extension of sphere and background ROIs, we decided to follow the approach of Furuie, [6], and then for each sphere and for each reconstruction parameter choice, we evaluated SA (Structural Accuracy) as:

$$SA = \sqrt{n_{sphere} n_{bkg}} \left(\mu_{sphere} - \mu_{bkg}\right) / \sqrt{n_{sphere}\sigma^2_{sphere} + n_{bkg}\sigma^2_{bkg}} \quad (5)$$

where n_{sphere} and n_{bkg} are the number of pixels of sphere ROI and background ROI respectively. SA was plotted against the update number; i.e. the number of iterations times the number of subsets. Average values of different combinations giving the same update number were considered in this regard. Optimal values for AWOSEM-REC and AWOSEM-NOREC were compared through their difference normalised by their average. This ensemble index is referred to as SA Ensemble Ratio (SAER) and permits to compare different algorithms at their best parameters choice.

Results

Spatial resolution for ECAT EXACT HR+ scanner is 4.6mm in the FOV centre and reaches, 25cm off axis, values larger than 6mm and 9mm in tangential and radial direction respectively.

It was generally observed that, set the update number, image quality slightly improves when iterations instead of subsets were increased. However, for summarising purpose, all the following results are presented versus image update number.

Sphere phantom: In Figure 1, an image of the sphere phantom (2Don7 acquisition) together with the ROIs displacement is shown.

ISSN: 1727-1983

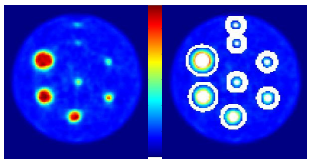

Figure1: Image of a transaxial slice of the sphere phantom and ROIs displacement.

As expected, the greatest contrast improvement due to LSF modelling took place for medium-small spheres, for off-axis acquisitions and at highest sphere to bkg activity ratio where the spill over effect is inferior. In Figure 2, CA versus image update number for 4.8 and 16.4mm spheres of 2Don7 acquisition is shown.

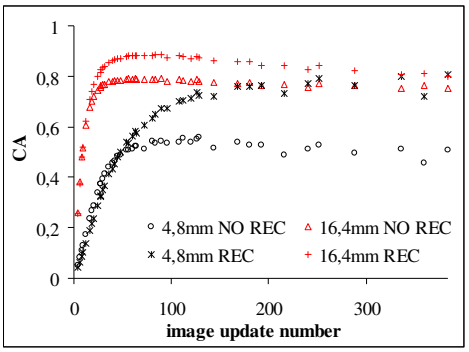

Figure 2: CA versus image update number for 4.8 and 16.4mm spheres of 2Don7 acquisition.

It's widely known that OSEM is characterised by an object dimension dependent resolution convergence rate [7]. Results in Figure 2 show that this phenomena is still observable when resolution recovery is introduced: convergence rate doesn't change and so the number of updates for CA convergence must be increased (mean increase of 50 updates over all the spheres). Looking at Figure 2, resolution recovery, at high image update number (>200), apparently seems able to obtain the same local contrast for small and big spheres; however results at such large updates are too much affected by noise breakup which alters image counts distribution.

NSR analysis confirmed that noise breakup effect is still present when resolution recovery is performed. In every condition of blurring or sphere to bkg activity ratio, NSR increases monotonically with image update number. However, as shown in Figure 3, NSR increasing rate is significantly reduced by resolution recovery, thanks to the blurring of terms composing image update. It's worth noting that, at high updates, the noise breakup looks quite different with and without resolution recovery. In AWOSEM-NOREC, noise produces hypo and hyperactive points all over the reconstructed image, making smallest spheres detection nearly impossible. In AWOSEM-REC the blurring of update terms limits also noise component maximum frequency, making hypo and hyperactivity more structured. Smallest spheres are then always well distinguishable, but false cold and hot spots appear on background and biggest spheres. Stopping rules and post-processing filters are then required even with resolution recovery.

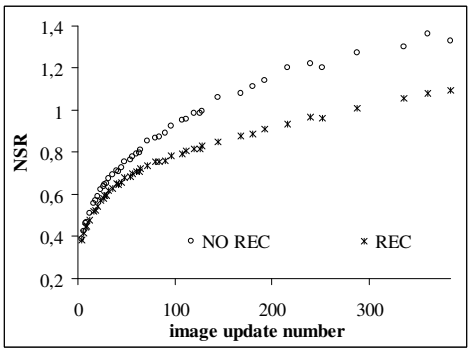

Figure 3: NSR versus image update number for 2Doff14 acquisition.

About SV, reconstructed objects non homogeneity, results have to be presented separately for large, medium and small spheres. In Figure 4 results for 4.8, 7.8, and 16.4mm spheres of 2Don7 acquisition are shown versus image update number.

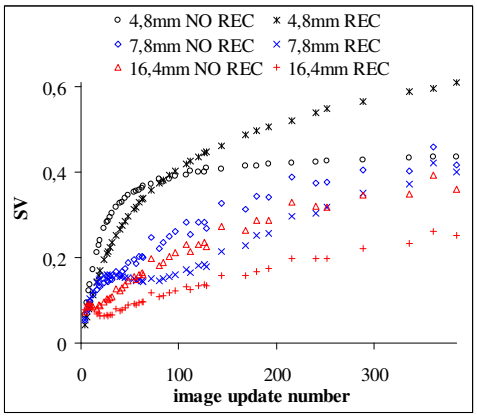

Figure 4: SV versus image update number for 4.8, 7.8, 16.4mm spheres of 2Don7 acquisition.

Looking at Figure 4: 1) for large spheres, to well define object structure and so to reach SV local minimum, only a small number of image updates is required. Resolution recovery, accordingly with CA results, moves SV minimum position slightly forward. After minimum is reached, SV increases for the noise breakup effect. 2) At smaller sphere radii, OSEM convergence rate reduction, together with partial volume effect, doesn't allow to reach a good object uniformity level before noise breakup onset. Then SV, in reconstructions obtained with AWOSEM-NOREC, is always monotonically increasing. When AWOSEM-REC is used, the SV local minimum become reachable also for medium radius spheres. 3) Things are different for very small spheres, where SV is, anyway, always increasing. In particular, for small update number, partial volume and noise

ISSN: 1727-1983

reduction due to resolution recovery globally improve homogeneity level. At higher updates, in spite of the great increasing of denominator term, SV for AWOSEM-REC is larger because of the algorithm tendency, for small-medium objects, to concentrate contrast recovery too much in sphere centre. The algorithm appears then unable to completely recover small object characteristics. At increasing blurring condition (off axis acquisitions) or at increasing sphere to background activity ratio, SV results are nearly the same obtained for 2Don7 acquisition.

Results about SA, Structural Accuracy, are represented in Figure 5 for three spheres of 2Don7 acquisition.

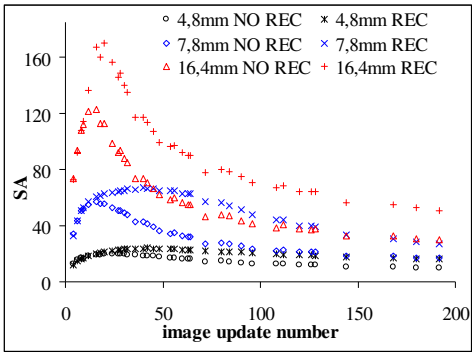

Figure 5: SA versus number of image updates for 4.8, 7.8, 16.4mm spheres of 2Don7 acquisition.

Data shown on Figure 5 confirm that resolution recovery is able to improve object characteristics, if image update numbers are properly chosen. SA is actually able to summarise information contained in the previously considered FOMs.

On this phantom, the effect of 2D Gaussian post-reconstruction filtering on SA was also evaluated (sigma ranging from 0.5 to 1.25*pixel size). For all the considered spheres and for both reconstruction methods, we found that the application of smaller sigma filters, reducing noise and object non homogeneity more than contrast, is able to enhance SA. For larger sigma values, the contrast loss amount becomes too much serious, thus decreasing SA. Globally, the best trade-off was obtained with sigma=pixel size for both the algorithms. Post-reconstruction filtering reduces the influence of update number on both the algorithm performances. Furthermore, the SA improvement and the optimal update number increase due to resolution recovery are generally reduced. In fact the contrast worsening amount is larger on AWOSEM-REC reconstructions, while noise reduction prevails on the AWOSEM-NOREC ones. However, where the partial volume effect is more important (i.e. small spheres, off axis acquisitions) the achievable structural accuracy enhancement due to resolution recovery is appreciable. SAER is shown in Table 2 for all the considered spheres.

Table 2: SAER value for each considered sphere.

	2Don14	2Don7	2Doff14	2Doff7
4.8mm	0.16	0.07	0.19	0.15
5.1mm	0.17	0.18	0.31	0.25
6.1mm	0.02	0.04	0.19	0.15
6.2mm	0.02	0.05	0.09	0.05
7.8mm	0.03	0.00	-0.02	-0.03
11mm	0.13	0.03	0.10	0.03
14mm	0.08	0.12	0.19	0.06
16.4mm	0.04	0.06	0.08	0.09

In Figure6, a transaxial slice of 2Doff14 phantom reconstructed with AWOSEM-REC and AWOSEM-NOREC is shown. For both the algorithms, small spheres SA optimal update number was used.

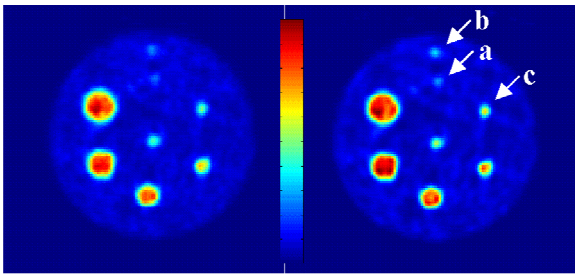

Figure 6: 2Doff14 phantom reconstructed with AWOSEM-NOREC 3it,12sub (left) and with AWOSEM-REC 4it,16sub (right). Images filtered with sigma=pixel size 2D Gaussian filter. Sphere diameter: a=4.8mm; b=5.1mm; c=6.1mm.

Alderson phantom, 2D mode: Because of the limited statistics, obtained results were slightly different for the two scans. Then results were averaged in order to extract more reliable quantities and conclusions. FOMs analysis were similar to the ones obtained on spheres phantom.

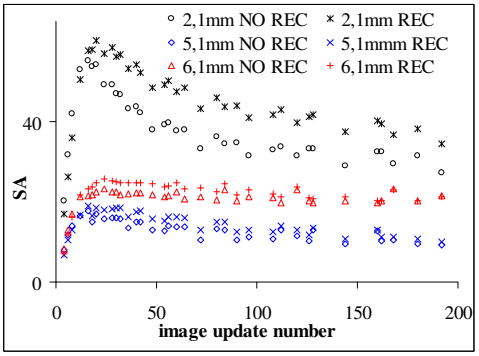

Figure 7: SA versus number of image updates for 2.1, 5.1, 6.1mm spheres of Alderson phantom (2D mode). SA was evaluated on data with 2D Gaussian post-filtering with sigma=pixel size.

Then, only summarising results about Structural Accuracy were reported. In Figure 7, SA values for 2.1,

ISSN: 1727-1983

5.1 and 6.1mm spheres after post reconstruction filtering (sigma=pixel size) are shown. In Table3, SAER, describing achievable Structural Accuracy improvement with resolution recovery, together with optimal update number for AWOSEM-REC and AWOSEM-NOREC, is reported for the five spheres.

Table 3: SAER and optimal update number for each considered sphere of the Alderson phantom 2D acquisition.

	SAER	NOREC update	REC update
2.1mm	0.09	16	20
4.1mm	-0.01	4	20
5.1mm	0.06	16	16
6.1mm	0.10	24	24
11.0mm	0.05	12	12

In Figure 8, reconstructions of the transaxial slice containing the 6.1mm sphere are shown.

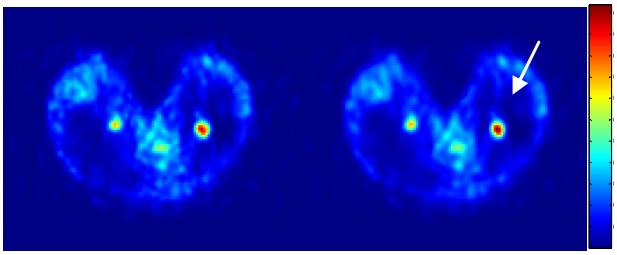

Figure 8: Transaxial slice of 2D Alderson phantom reconstructed with AWOSEM-NOREC (left) and with AWOSEM-REC (right). Both images were obtained with 3it,8sub and filtered with sigma=pixel size 2D Gaussian filter. Sphere diameter: 6.1mm.

Alderson phantom, 3D mode: Also for 3D mode acquisition, results of two consecutive scans were averaged and only results about Structural Accuracy were reported. In Figure 9, SA for 2.1, 5.1 and 6.1mm spheres after post reconstruction optimal filtering (sigma=pixel size) is shown.

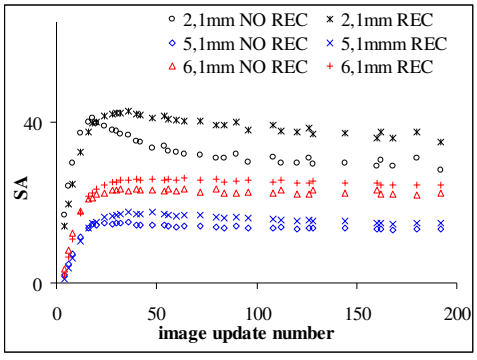

Figure 9: SA versus number of image updates for 2.1, 5.1, 6.1mm spheres of Alderson phantom (3D acquisition). SA is evaluated on data after 2D Gaussian post-filtering with sigma=pixel size.

In table 4, SAER and optimal update number are reported for the five spheres.

Table 4: SAER and optimal update number for each considered sphere of the Alderson phantom 3D acquisition.

	SAER	NOREC update	REC update
2.1mm	0.04	18	36
4.1mm	-0.02	8	12
5.1mm	0.15	36	36
6.1mm	0.10	40	40
11.0mm	0.03	12	12

In Figure 10, reconstructions of the transaxial slice containing the 6.1mm sphere are shown.

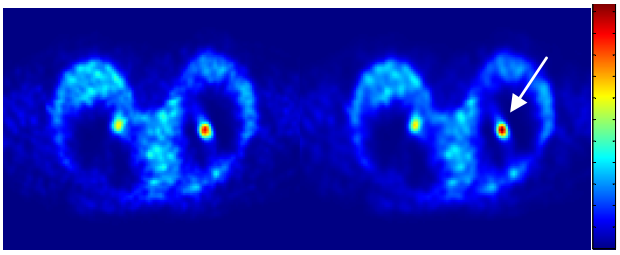

Figure 10: Transaxial slice of 3D Alderson phantom reconstructed with AWOSEM-NOREC (left) and with AWOSEM-REC (right). Both images were obtained with 5it,8sub and filtered with sigma=pixel size 2D Gaussian filter. Sphere diameter: 6.1mm.

Discussion and conclusions

In PET studies, small lesion detectability and quantification accuracy are limited by the large noise component and by partial volume and spill over effects. Usually, in clinical practice, to obtain an adequate image quality, post reconstruction filtering is performed, thus further augmenting the blurring amount. Some improvement is needed, mostly to increase accuracy of oncological studies in which small lesions have to be detected, measured, and up followed. In this work we wanted to verify the performance of resolution recovery within iterative reconstruction in achieving these goals. Therefore, reconstructions of phantoms with known geometry and activity, thus reproducing some of possible clinical scenarios, were analyzed. The proposed algorithm, AWOSEM-REC, and the standard one, AWOSEM-NOREC, were compared on spheres of different size, activity to background ratio and off-axis displacement. Furthermore, reconstruction were compared over wide parameter ranges, varying iteration number, subset number, and 2D Gaussian filter sigma. In a first analysis the post-filtering was not considered; in successive analysis it was introduced. For every considered sphere, all the aspects influencing lesion detectability and quantification accuracy were taken into consideration. Contrast accuracy, object uniformity and background noise amount were then measured.

ISSN: 1727-1983

The analysis carried out without post-filtering showed that:

1) On medium-large spheres the resolution recovery introduction succeeded in making achievable a better contrast and uniformity condition. In fact the algorithm allows to well define object structure before the noise breakup onset. Hence, an useful parameter range can be determined, with a number of updates sufficient to perform resolution recovery, but below the appearance of the characteristic structured noise breakup on uniform activity regions.

2) On small spheres the convergence rate was lower and furthermore, at high updates, the algorithm acted too much concentrating activity in sphere centre. Hence, contrast optimality can not be reached and a compromise between noise and accuracy must be found. Results obtained were however relevant: the compromise solution of AWOSEM-REC was largely better than the one of AWOSEM-NOREC. Contrast increase and background noise reduction both improved lesion detectability.

It must be also observed that, without post-filtering, the optimal update range was quite narrow and often not overlapped for different sphere size, activity, and position.

The introduction of post-reconstruction filtering was able, for both algorithms, to improve image quality and global Structural Accuracy. After post-filtering, optimal update number choice became less critical too, and differences between AWOSEM-REC and AWOSEM-NOREC appeared to be reduced. In fact the filter partially destroyed the recovered contrast on AWOSEM-REC images and, conversely, decreased the noise component, which was prevailing on AWOSEM-NOREC images. As a consequence, resolution recovery improvements were no more appreciated on medium-large objects (>6 mm) of the sphere phantom, characterised by a count statistics level more than clinical and by an uniform background. In fact, the contrast increase due to resolution recovery was not uniform inside the object, thus leading to the same Structural Accuracy obtainable with AWOSEM-NOREC which reconstructs more blurred but uniform objects. However, the effect of resolution recovery appeared important where the blurring effect was more critical, i.e. on small spheres, particularly off axis. AWOSEM-REC, reducing background noise and better defining object structure and contrast, succeeded in increasing lesion detectability. A large contrast improvement on this kind of sphere can't be reached because it would require a large number of update characterised by false spot appearance.

The Alderson thorax-abdomen phantom, was scanned at a clinical count statistics level and its activity distribution was more similar to oncological patient FDG uptake. Furthermore, results on this phantom were averaged over two consecutive acquisitions, thus increasing their significance. In this condition, resolution recovery succeeded in improving accuracy in most instances. In fact AWOSEM-REC was able to delay the noise breakup onset, thus making a contrast improvement achievable, both in 2D and in 3D acquisition mode. As to reconstruction parameters, the update number to Structural Accuracy optimality with AWOSEM-REC increased on small spheres and didn't change on large ones. In 3D acquisition, due to the larger data Signal to Noise Ratio, parameter choice appeared simpler.

In conclusion, the optimisation of iterative reconstruction algorithms for clinical purposes has to face the trade-off between blurring reduction and noise effects. Extensive studies over reconstruction modalities and parameters can provide valuable indication for the choice of protocols best performing as to lesion detectability and evaluation.

References

[1] QI J., LEAHY R.M., HSU C., FARQUHAR T.H. and CHERRY S.R. (1998): 'Fully 3D Bayesian reconstruction for the ECAT EXACT HR+', *IEEE. Trans. Nuc. Sci.*, **45(3)**, pp. 1096-1103

[2] HUDSON H.M. and LARKIN R.S. (1994): 'Accelerated image reconstruction using ordered subsets of projection data', *IEEE. Trans. Med. Imag.*, **13(4)**, pp. 601-609

[3] DE BERNARDI E., ZITO F., MICHELUTTI M., MAINARDI L., GERUNDINI P. and BASELLI G. (2003): 'Improving PET image spatial resolution by experimental measurement of scanner blurring properies', Proc. of 25th Ann. Conf. IEEE – EMBC 2003, Cancun, Mexico, p 975-977

[4] BUTTI M., DE BERNARDI E., ZITO F., MAINARDI L., CERUTTI S., GERUNDINI P. and BASELLI G. (2004): 'Applying 2D ML iterative reconstruction methods with resolution recovery to 3D PET data: evaluation of rebinning effects', Proc. of 26th Ann. Conf. IEEE –EMBC 2004, San Francisco, USA, p 1365-1367

[5] DEFRISE M., KINAHAN P.E., TOWNSEND D.W., MICHEL C., SIBOMANA M. and NEWPORT D.F. (1997): 'Exact and approximate rebinning algorithms for 3D PET data', *IEEE. Trans. Med. Imag.*, **16(2)**, pp. 145-158

[6] FURUIE S.S., HERMAN G.T., NARAYAN T.K., KINAHAN P.E., KARP J.S., LEWITT R.M. and MATEJ S. (1994): 'A methodology for testing for statistically significant differences between fully 3D PET reconstruction algorithms', *Phys. Med. Biol.*, **39**, pp. 341-354

[7] LIOW J.S. and STROHER S.C. (1993): 'The convergence of object dependent resolution in maximum likelihood based tomographic image reconstruction', *Phys. Med. Biol.*, **38**, pp. 55-70

ISSN: 1727-1983